ELSEVIER

Journal of Marine Systems 18 (1998) 287–312

JOURNAL OF MARINE SYSTEMS

A seasonal three-dimensional study of the nitrogen cycle in the Mediterranean Sea Part I. Model implementation and numerical results

A. Crise *, G. Crispi, E. Mauri

Osservatorio Geofisico Sperimentale, P.O. Box 2011, 34016 Trieste, Italy

Received 1 February 1996; accepted 4 November 1997

Abstract

The influence of the general circulation on the lower trophic level variability in the Mediterranean is investigated by means of a three-dimensional coupled hydrodynamical ecological model. While the hydrodynamical forcing is obtained by a primitive equation seasonal model, the trophic dynamics are described using an aggregated model based on inorganic nitrogen, phytoplankton and detritus. The model results exhibit a quasi-repeating seasonal cycle and the calculated fluxes through the principal straits are of the same order as those estimated from literature data. The climatological influence of the general circulation on the nutrient distribution is evident in permanent cyclonic areas, while the anticyclonic circulation does not give a detectable signal, due to the high oligotrophy of the upper layer. The seasonal cycle shows marked spatial differences according to the different regimes induced by the surface circulation, leading to the tentative conclusion that, in the upper layer, the circulation directly or indirectly determines the distribution of the dissolved inorganic nitrogen concentration.

Keywords: phytoplankton; inorganic nitrogen; seasonal cycle

1. Introduction

It is widely accepted that the distribution of biological production in ocean basins is correlated with the presence of general circulation and mesoscale features [for an overview, see the work of Mann and Lazier (1991)]. Less effort has been paid to modelling lower trophic level dynamics on a basin scale, and explicitly taking into account the influence of the hydrodynamical forcings on ecosystem function (Sarmiento et al., 1993; Najjar et al., 1992; Fasham et al., 1993).

The Mediterranean appears to be a natural candidate for such studies being a semi-enclosed basin in which all the relevant processes that govern ocean circulation are present, but on a smaller scale, and where trophic conditions vary from mesotrophic to extremely oligotrophic. Nevertheless, the lack of comprehensive datasets, the paucity of long biogeochemical time series and the low level of knowledge on the forcings has prevented an attack on this problem up to now.

In recent years, a substantial improvement in knowledge has been obtained through international

* Corresponding author.

0924-7963/98/$ - see front matter
PII: S0924-7963(98)00016-5

cooperative programs that have helped to make large quantities of new data and models calibrated for the Mediterranean and its subbasins available.

Taking advantage of this renewed interest, the aim of this study is a modelling of the general circulation influence on the seasonal nitrogen cycle throughout the Mediterranean Sea, resolving subbasin scales features and their time evolution.

As a first guess, the complexity of the problem cannot be approached, as in regional marine ecosystem modelling, as done for the North Sea (Baretta et al., 1995). Such modelling effort is based on a large, comprehensive dataset that can be used to calibrate and validate the biomass-oriented scheme described by more than 50 state variables connected by over hundred parameters. This model takes advantage of the relatively simple dynamics of the North Sea, described by means of a box model. The conditions in Mediterranean are completely reversed: the known oligotrophy and the prominent seasonal cycle in the forcings, typical of the mid-latitudes, concur in creating a dynamical environment where physical processes play a crucial role in conditioning the ecosystem function. Moreover, the scarcity of available dataset prevents any reasonable attempt to calibrate detailed, deterministic models describing the whole food chain from autotrophs to fishes. We use therefore a more aggregated description, where determination of the scales at which the ecosystem response is sensitive to the physical forcings will help in defining which processes have to be explicitly included and which have to be parametrized or left out.

In Section 2, the aggregated coupled model is discussed on the basis of a scale analysis. A description of the model, of the chosen parametrization and initial conditions are then examined. Some theoretical considerations about a simplified formulation of the equation-set lead to the conclusion that the NPD model is able to determine phytoplankton persistence on the basis of irradiance and nutrient availability.

The model results are described in Section 3, showing the quasi-repeating seasonal cycle and the fluxes through the principal straits. The climatological influence of the general circulation is also evidenced, as well as the effects of the seasonal cycle.

Finally, in Section 4 the overall conclusions are drawn and an overview of future work is given.

Although Mediterranean datasets do not allow a calibration of a basin-wide trophic model, an attempt to link models with observations is made in order to support the confidence in the numerical results. The companion paper by Crispi et al. (1999) (henceforth CCM-2) is focused on model verification. In situ and remotely sensed data are used to confirm both spatial variability and seasonal phytoplankton response to the nutrient inport/export induced by the general circulation.

2. Description of the model

An ocean general circulation model (OGCM) is the most appropriate for describing the annual variability and interannual modulation of the mean flow field for basin-wide simulations. For the Mediterranean the typical time scale (for the surface layer) is:

$$t_{gc} = \frac{L_{med}}{|v|} = \frac{O[10^6]\mathrm{m}}{O[10^{-1}]\mathrm{m\,s^{-1}}} = O[10^7\mathrm{s}] = O[\mathrm{month}] \quad (1)$$

where t_{gc} is the time scale typical of the whole basin, L_{med} is the typical length and $|v|$ is the typical module of the horizontal velocity. For subbasin features the typical time scale can be assumed to be:

$$t_{sub} = \frac{L_{sub}}{|v|} = \frac{O[10^5]\mathrm{m}}{O[10^{-1}]\mathrm{m\,s^{-1}}} = O[10^6\mathrm{s}] = O[\mathrm{week}] \quad (2)$$

On the other hand, the scales involved in a description of a mixed layer model of the nitrogen cycle (Fasham et al., 1990) are shown in Fig. 1 in the abscissa, a logarithmic scale is used for explicit reference on the time scale of each process. We see that the degradation transitions from biota into detrital forms have characteristic times of the same order as those calculated for the subbasin features in Eq. (2). For the other processes, the influence of the general circulation is not relevant when time and space scales differ by many orders of magnitude, and it is known that small-scale ecosystem dynamics are

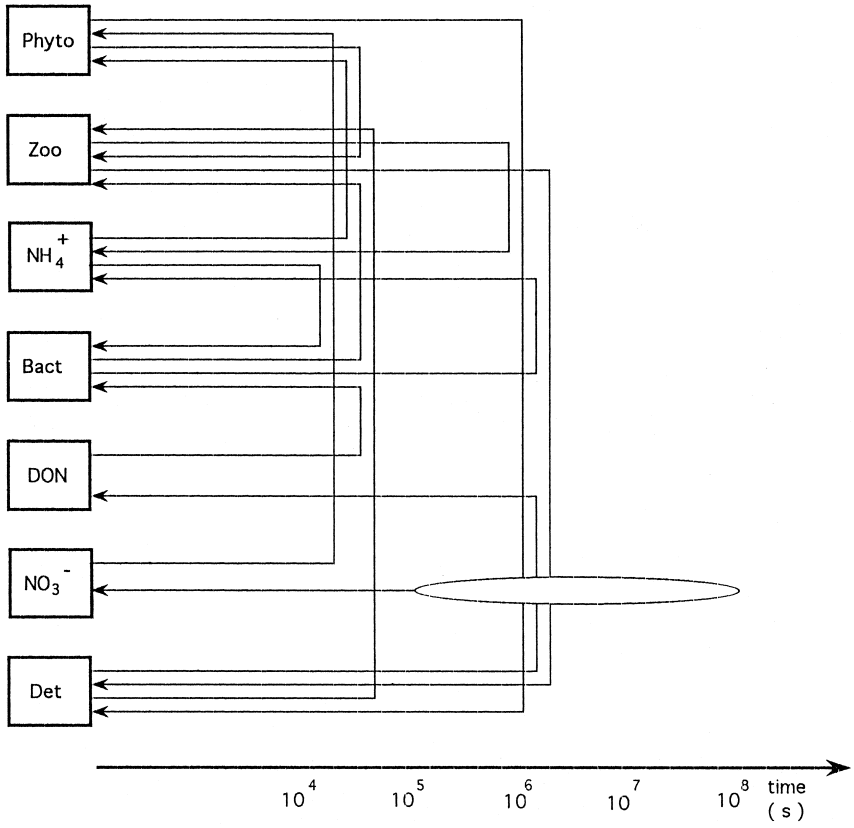

Fig. 1. Time referenced flow diagram of the nitrogen cycle [from the work of Fasham et al. (1990), redrawn].

dominated firstly by turbulent and then by viscous processes.

At mid-latitudes, the seasonal cycle of the nutrients is connected with the nutrients transported into the photic zone or included within the productive layer by the seasonal deepening of the compensation depth (for definition, see Section 2.3), where it is transformed into new production. For elementary stationarity considerations, at equilibrium, the net balance of detritus flux must compensate the integral of new production,on an annual average (Eppley and Peterson, 1979).

For these reasons, an aggregated ecological model able to reproduce the nutrient dynamics seems to be sufficient as a first guess at a description of the trophic response to the physical forcings,and further analytical details, presented in Section 3, will support this statement.The ecological model needs to be tightly coupled with the OGCM in order to benefit from the full resolution of the physical forcings.

2.1. The ecological equations

The aggregated trophodynamic nitrogen model describes the nitrogen cycle by giving the space and time evolution of three large compartments, N, P and D, that schematically represent the above medium-to-long term processes: N represents the dissolved inorganic nitrogen, P is the phytoplankton biomass nitrogen equivalent and D those organic forms that span from DON to macro aggregates. In this stage, zooplankton is implicitly considered: in an oligotrophic environment microzooplankton can be incorporated in the phytoplankton compartment because the forcings time scales (‘perpetual year’ monthly means) and the model response cannot resolve high frequency processes connected by the

regenerated production (Anderson et al., 1993). Mesozooplankton is difficult to be explicitly considered in a coupled model because the overwintering and feeding strategies cannot be represented as a simple biological tracer (Broekhuizen et al., 1995). On the other hand, zooplankton parametrization uncertainties and errors affect not only the upper trophic level, but the whole system steady state (Fransz et al., 1991). The possible overestimation of phytoplankton concentration affects the model prognosis, but it slightly alters the statistics (scatter plots, regressions) and the differential entities (fluxes), which constitute the basis of our results analysis.

The choice of nitrogen as limiting factor can be seen as realistic in the Western Mediterranean, while in the Levantine basin there is some experimental evidence that phosphorous acts as primary production limitator (Berland et al., 1988), and thus in that basin we could have an overestimation of the primary production. The trophodynamic model is basically composed of three diffusion—advection reaction equations that will be discussed in detail in the following sections.

2.1.1. Phytoplankton equation

All the autotrophic forms are included in one compartment which blends the trophic characteristics of ultraplankton and microplankton:

$$\frac{\partial P}{\partial t} = -(\vec{u}\cdot\nabla)P - K_{\mathrm{H}}\Delta_{\mathrm{h}}^2 P + K_{\mathrm{V}}\frac{\partial^2 P}{\partial z^2} + F(T,\bar{I},N)P - dP, \quad (3)$$

where $\vec{u}$ is the prognostic velocity and Δ_{h} is the horizontal Laplace operator. $F(T,I,N)$ denotes the phytoplankton growth rate dependent on temperature, nitrogen concentration and irradiance, and d the phytoplankton mortality and respiration rate. The Michaelis–Menten nutrient limitation for algal growth is formulated as follows:

$$F(T,\bar{I},N) = g(T)L(\bar{I})\frac{N}{C_{\mathrm{N}}+N} \quad (4)$$

where C_{N} is the half-saturation constant for nitrogen. The temperature dependency term $g(T)$ is computed using the Arrhenius' formulation (Eppley, 1972):

$$g(T) = G_{\max}e^{k_T T} \quad (5)$$

The light limitation formula $L(\bar{I})$ is:

$$L(\bar{I}) = rf\frac{\bar{I}}{I_{\mathrm{opt}}}e^{1-\frac{\bar{I}}{I_{\mathrm{opt}}}} \quad (6)$$

where the optimum light I_{opt} is chosen to be $I_0/2$, in agreement with Steele (1962).

We used two formulations in the implementation of the irradiance formula: for the normalized daylength rf the first one assumes a zonal independency, being function on time only:

$$rf(\mathrm{day}) = f_1 + f_2\cos\left(\frac{2\pi(\mathrm{day}+10)}{360}\right) \quad (7)$$

where day is the julian day of a 'reduced' 360 days year. The depth dependent irradiance $\bar{I}$ is calculated exploiting the Lambert–Beer law:

$$\bar{I} = I_0 e^{-k_z z}$$

where I_0 is the scalar irradiance at surface. This formulation used in a daily integrated cycle basically eliminates the need for estimation of the photosynthetic active ratio (PAR): the $\bar{I}/I_{\mathrm{opt}}$ ratio is independent of the fraction of total irradiance present in the photosynthetic active band.

A second, improved, light model based on a non-spectral formulation of the irradiance was developed consistently with the physical model, including a spatial dependence on the extinction coefficient, phytoplankton selfshading and cloud effects. In particular, light extinction in the water column was assumed to be dependent on the zonally variant extinction coefficient and on the phytoplankton concentration (selfshading):

$$\bar{I} = I_0' e^{-k_z z - k_{\mathrm{phyto}}\int_0^z P\,\mathrm{d}z} \quad (8)$$

where k_z is the light extinction coefficient and k_{phyto} is the selfshading factor. Another factor relevant to the spatial and temporal modulation of the light forcing is the surface irradiance dependence on normalized cloud coverage cl derived by COADS dataset (Castellari et al., 1990), following the empirical formulation of Reed (1977):

$$I_0' = I_0(1 - 0.62\,\mathrm{cl} + 0.0019\,\mathrm{sunbeta}) \quad (9)$$

where sunbeta is function of the sun zenith angle. In this case, the normalized day-length rf to be intro-

duced in Eq. (6), is calculated using the Brock (1981) method:

$$rf = \text{daylength}/\pi = \arccos(-tg(\text{declination}) \times tg(\phi))/\pi \quad (10)$$

where ϕ is the latitude in radiant. The sun declination is calculated as follows:

$$\text{declination} = -0.406\cos(2\pi(\text{day}+10)/360) \quad (11)$$

relying on the simplifying hypothesis of a circular Earth orbit around the Sun (Forsythe et al., 1995).

2.1.2. Detritus equation

The detritus equation parametrizes different functional groups that include the non-living part of PON and DON. The detrital pool receives contributes through the phytoplankton loss rate d, derived from cell respiration and lysis, and through remineralization r, regenerates dissolved inorganic nitrogen:

$$\frac{\partial D}{\partial t} = -(\vec{u}\cdot\nabla)D - w_D\frac{\partial D}{\partial z} - K_H\Delta_h^2 D + K_V\frac{\partial^2 D}{\partial z^2} - rD + dP \quad (12)$$

The vertical sinking is simulated by a vertical velocity constant along the water column. A careful estimation of the detritus vertical flux is extremely important for an overall productive zone budget determination. In terms of vertical transport, the falling particles can be operationally grouped into three categories: fecal pellets, aggregates, and dissolved organic matter (at least the labile part should be taken into account). The last fraction makes a small contribution to the gravity-driven D flux because of its neutral buoyancy. They have different remineralization rates, depending on external conditions (temperature, pressure), and the ultimate fate of the nitrogen content is influenced by recycling in the productive zone under different states before sinking. Nevertheless, using Mediterranean literature data for all these D-forms, a regeneration time scale $O(10$ days) has been obtained and an averaged sinking velocity of $O(5$ m day$^{-1})$ estimated (Mauri and Crise, 1995). These values, assigned respectively to r and w_D, were used in run b.10 and following ones (see Table 2).

2.1.3. Dissolved inorganic nitrogen equation

In this compartment are included all the inorganic forms of nitrogen creating a nutrient pool which is made available to the phytoplankton uptake:

$$\frac{\partial N}{\partial t} = -(\vec{u}\cdot\nabla)N - K_H\Delta_h^2 N + K_V\frac{\partial^2 N}{\partial z^2} - F(T,N,I)P + rD \quad (13)$$

For the sake of simplicity, in this equation the external sources and sinks are not mentioned (discussion of the Gibraltar budget parametrization will be carried out in Section 2.2). The riverine input is disregarded for the moment in the model; this can be justified basically by the fact that the Nile is dammed and the effects of runoff are quite local (Azov, 1986); the Po and Adriatic river discharges do not seem to affect exchange with the Mediterranean, possibly because of the trapping effect on nutrient distribution (Poulain et al., 1996) due to the shelf benthic processes; and the Rhone only seems to make relevant contributions of nitrates (0.082×10^6 tm^{-2}) and Kjerdal nitrogen (0.050×10^6 tm^{-2}), according to Tusseau and Mouchel (1995), but these values are quite small in comparison with the values at Gibraltar and Sicily Straits reported in Table 3.

2.1.4. Boundary conditions and convection parametrization

The no-flux conditions for this set of equations are obtained with the vanishing of the normal gradients of all biological state variables at the boundaries:

$$\frac{\partial b}{\partial n} = 0$$

Here, b is a generic biological tracer and n is the coordinate normal to the wall. The biharmonic parametrization of the turbulent eddy diffusivity needs an additional boundary condition:

$$\frac{\partial(\Delta_h b)}{\partial n} = 0$$

In the case of water column instability, the convective adjustment is obtained by an instantaneous vertical mixing applied to all the tracers, repeating the mixing up to five times if necessary. The convec-

tion contemporarily acts on both biochemical and physical tracers.

2.2. Initial conditions and ecological parameters

Within the NPD framework, an attempt was made to develop a better and more general parametrization of vertical biology-controlled nitrogen transport processes. A correct estimate of nitrogen fluxes needs a realistic initialization of the DIN: since nitrates are by far the largest fraction of the DIN (at least in the ocean interiors) it is initialized with nitrate vertical profiles typical for each subbasin, as shown in Fig. 2. This stepwise initializing function was smoothed using an order three moving average filter.

The profile of the phytoplanktonic biomass used for initialization of the model is worked out from the chlorophyll a measured in the Ionian Sea during the POEM-BC-O91 cruise in October 1991. The chlorophyll values, mg Chla m^{-3} are converted to biomass mg C m^{-3} by means of the relation C:Chla = 24 given by Gould and Wiesenburg (1990) for the Western Mediterranean Sea, taking the average of this ratio from the 80 m profile in November. The biomass values are obtained using the Redfield et al. (1963) ratio.

The detritus initial profile is chosen as null everywhere. After the spin-up it reaches its quasistationary equilibrium inside the basin.

The overall parameters used for the NPD model are reported in Table 1. The light attenuation coefficient relies on POEM-BC-O91 Secchi disk data (Kovacevic et al., 1994) after an averaged postprocessing of the Ionian data.

To simulate the nitrogen inflow/outflow through the Gibraltar Strait a representation of the nutrient exchanges is implemented using an Atlantic box extending from 5.5 W to 9.5 W. In this buffer zone, a Newtonian relaxation to values typical of the upper Atlantic layer for all three state variables (inorganic nitrogen, phytoplankton and detritus) is imposed.

For relaxation of nitrate in the Atlantic box of the model we used the data from the ATLANTIS II cruise (Osborne et al., 1992). For phytoplankton the

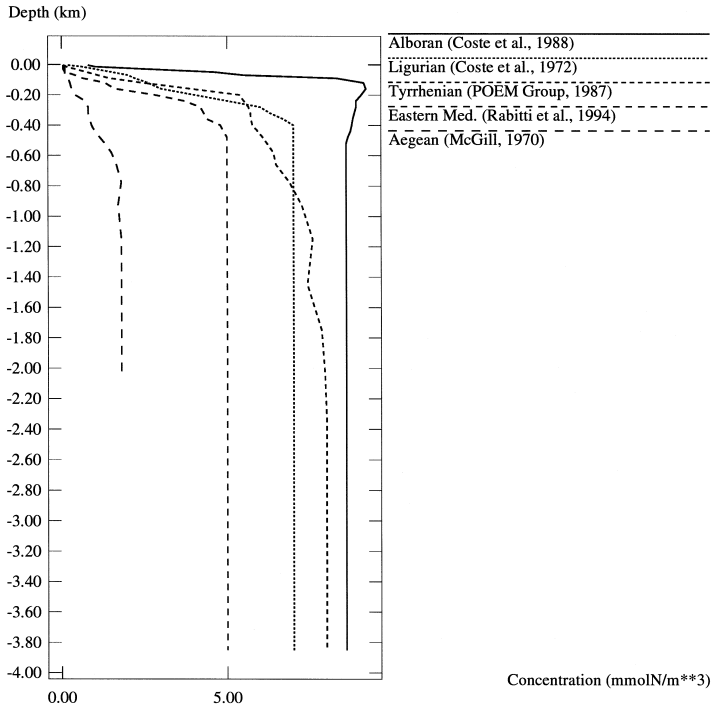

Fig. 2. Measured NO_3 profiles used to generate basin-dependent initial conditions for DIN concentrations. (Data from McGill, 1970; Coste et al., 1972, 1988; POEM Group, 1987; Rabitti et al., 1994.)

Table 1
Parameters used for the standard NPD ecomodel

Parameter	Definition	Unit	Value	Reference
C_N	Nitrate half-saturation	mgatN m^{-3}	0.25	MacIsaac and Dugdale (1969)
d	Phytoplankton mortality	s^{-1}	5.55×10^{-7}	Slagstad (1982)
G_{max}	Maximum growth rate	s^{-1}	6.83×10^{-6}	Eppley (1972)
τ	Regeneration rate	s^{-1}	1.19×10^{-5}	calibration
w_D	Detritus sinking velocity	cm s^{-1}	-0.0012	calibration
k_T	Temperature coefficient	$°C^{-1}$	6.33×10^{-2}	Eppley (1972)
k_z	Light attenuation	cm^{-1}	0.0005	POEM-BC-O91
k_{phyto}	Self-shading coefficient	m^2 mgatN^{-1}	0.	calibration
I_{opt}/I_0	Optimum light ratio		0.5	Steele (1962)
f_1	Photoperiod add. coef.		0.5	UNESCO (1983)
f_2	Photoperiod mul. coef.		0.125	UNESCO (1983)
K_H	Horizontal diffusion	$cm^4\ s^{-1}$	0.2×10^{19}	calibration
K_V	Vertical diffusion	$cm^2\ s^{-1}$	1.5	calibration

same profile used for initialization inside the basin is used for relaxation in the buffer zone. Detritus relaxation to zero is assumed for the whole Atlantic zone, with a time constant of 5 days, as for the other variables. The profiles used for restoring the inorganic nitrogen and the phytoplankton in the Atlantic buffer zone are shown in Fig. 3.

The phytoplankton first level values are also relaxed to the initial profile value P^0 at surface with a time constant R of 5 days:

$$P' = P - R(P - P^0) \tag{14}$$

where P is the prognostically evaluated phytoplankton in the generic grid point of the first level and P' is the relaxed value. To ensure the tracer conservativeness a balancing term in the detritus compartment is introduced:

$$D' = D + P' - P \tag{15}$$

where D' is the modified detritus concentration. Using staggered finite differences it is possible to have negative concentrations where strong lateral or vertical gradients are present (Sarmiento et al., 1993). This wiggling effect is overcome here with the following borrowing technique:

$$X_i = 0;\ X_{\mathrm{mod}(i+1,3)} = X_{\mathrm{mod}(i+1,3)} + X_i \text{ if } X_i < 0, \tag{16}$$

$$X_i = X_i; \text{ if } X_i \geq 0, \tag{17}$$

where X_i, $i = 1,2,3$ are respectively DIN, phytoplankton and detritus in that order. The FORTRAN-like symbols $X_{\mathrm{mod}(i+1,3)}$ used for the index mean that when negative values occur for a variable the compensation is obtained cyclically by borrowing the needed amount of nitrogen equivalent from the successive state variable. This technique has the property that if a total negative balance is obtained the phytoplankton and detritus compartments are set to zero and the negative value is assigned to the DIN of the overall nitrogen concentration. The absence of a source term in the DIN Eq. (6) dependent on DIN itself does not propagate the instability in time and space, thus leaving to the diffusion term of the equation the task of reestablishing realistic values for all three state variables.

2.3. Analytical results

An analytical discussion of the equation set describing the nitrogen cycle dynamics can give important insights into some of the system dynamic characteristics, even though a more rigorous treatment will be left to a forthcoming paper. Under the simplifying hypothesis of lateral and vertical homogeneity, and in absence of relaxation the Eqs. (13), (3) and (12) can be rewritten as a NPD equation set:

$$\frac{dN}{dt} = -G_{TI}N/(C_N + N)P + rD \tag{18}$$

$$\frac{dP}{dt} = G_{TI}N/(C_N + N)P - dP \tag{19}$$

$$\frac{dD}{dt} = dP - rD \tag{20}$$

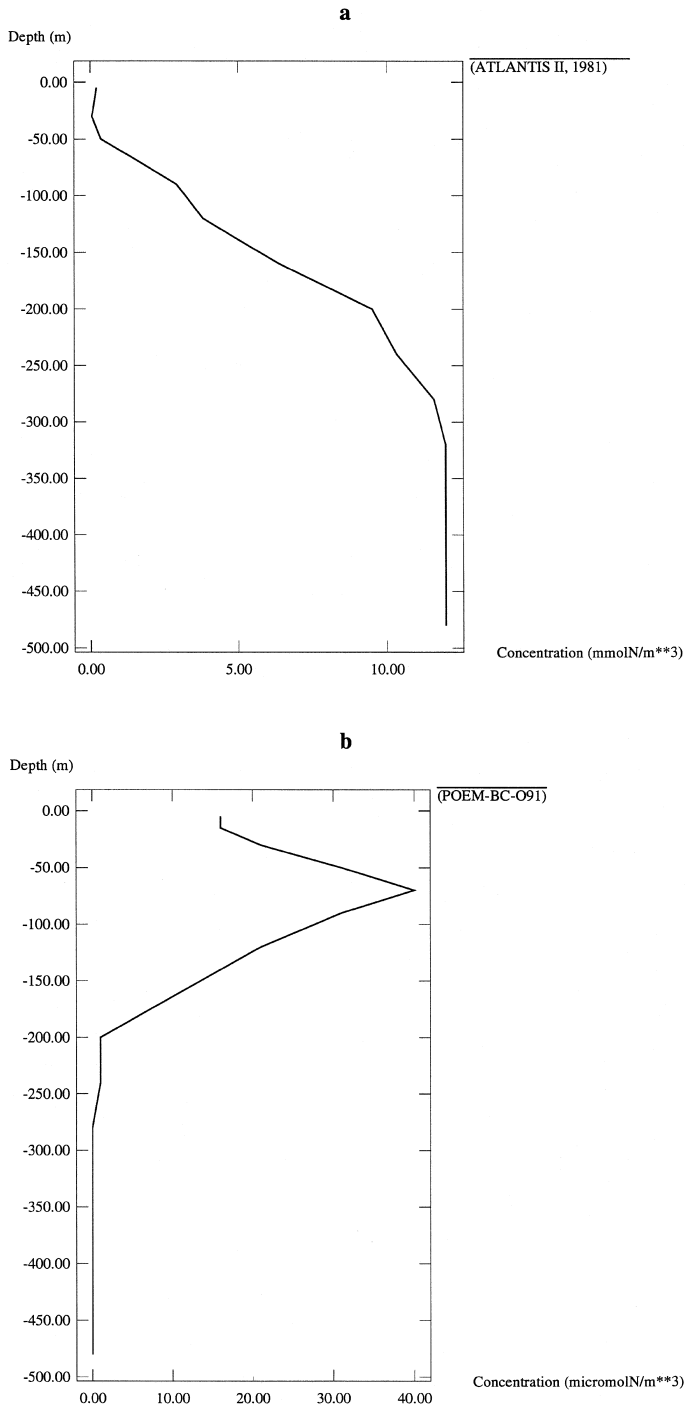

Fig. 3. (a) NO_3 profile used as restoring condition for DIN in the Atlantic box. (b) Average initial and restoring profile used in the whole model domain to initialize, and in the Atlantic box to restore, the phytoplankton concentration.

where G_{TI} is the average of the contribution of temperature and light terms to the growth rate along the year:

$$G_{TI} = \frac{1}{\text{year}} \int_{\text{year}} g(T)\, L(T) \mathrm{d}t.$$

Summing the N, P, and D equations, we obtain:

$$\frac{\mathrm{d}\sum N}{\mathrm{d}t} = 0, \tag{21}$$

where:

$$\Sigma N = N + P + D \tag{22}$$

giving the conservativeness of the total nitrogen. This result can be extended to the full 3D coupled model when Gibraltar and other possible sources/sinks are disactivated (Crise et al., 1992). Exploiting the conservation closure (Eq. (22)) the NPD system can be reduced to a two-dimensional autonomous (i.e., non-explicitly time-dependent) system of ODE. This system admits no more than two equilibria, depending on the parameter choice. A trivial equilibrium solution is possible when all the nitrogen is present in inorganic form only:

$$N_{e1} = \sum N;\ P_{e1} = D_{e1} = 0$$

The other equilibrium solution is:

$$N_{e2} = \frac{dC_{\mathrm{N}}}{G_{TI} - d} \tag{23}$$

$$P_{e2} = \frac{r}{d + r}(\sum N - N_{e2}) \tag{24}$$

$$D_{e2} = \frac{d}{d + r}(\sum N - N_{e2}) \tag{25}$$

Under the condition:

$$N, P, D \geq 0$$

for the second equilibrium, the following inequality always holds:

$$\sum N > N_{e2}$$

Thus, we can rewrite Eq. (23) as an inequality condition on the phytoplankton persistence at equilibrium:

$$Gd(1 + C_{\mathrm{N}}/\sum N) \tag{26}$$

An analysis of this condition leads to identification of two possible scenarios: the eutrophic and the oligotrophic regimes. In the eutrophic limit ($\sum N \gg C_{\mathrm{N}}$), we obtain the result that the phytoplankton survival is guaranteed within the annual averaged compensation depth, i.e., the depth where the phytoplankton growth (basically light-limited and temperature dependent) compensates the losses (mortality and respiration) on an annual basis. The compensation depth can be evaluated by simply finding the depth zc where (in the absence of nutrient limitation) the following integral relation holds:

$$\int_0^{zc} \int_{\text{year}} G_{TI} P \mathrm{d}t \mathrm{d}z = \int_0^{zc} \int_{\text{year}} dP \mathrm{d}t \mathrm{d}z G_{TI}$$

Because of the supposed homogeneity we have:

$$\int_{\text{year}} (G_{TI} - d) P \mathrm{d}t = 0.$$

P is by definition positive, and thus:

$$G_{TI} - d = 0.$$

This result is exactly the lower boundary for inequality (Eq. (26)) in the eutrophic limit: the ecosystem is thus strongly light-limited. In the oligotrophic limit ($C_{\mathrm{N}} \gg \sum N$) the growth rate must be larger than the nutrient dependent term in Eq. (26); the C_{N}–total nitrogen availability ratio is larger than one and the conditions for phytoplankton survival are much more severe in comparison with the eutrophic regime. This equilibrium also takes into account the fact that in oligotrophic waters small-sized small-C_{N} cells can survive better than larger and slower growing ones: the restrictions on phytoplankton persistence in the oligotrophic limit are relaxed by the presence at the denominator of low values of the half saturation constant C_{N}. This numerical result is supported also by observations: the Levantine basin, which is considered to be highly oligotrophic, exhibits a larger picoplankton presence, constituting between 70% and 82% of the total chlorophyll all over the year (Berman et al., 1986; Berland et al., 1988). Armstrong (1994) numerically demonstrated that smaller algal classes dominate in oligotrophic conditions, larger size phytoplankton being added

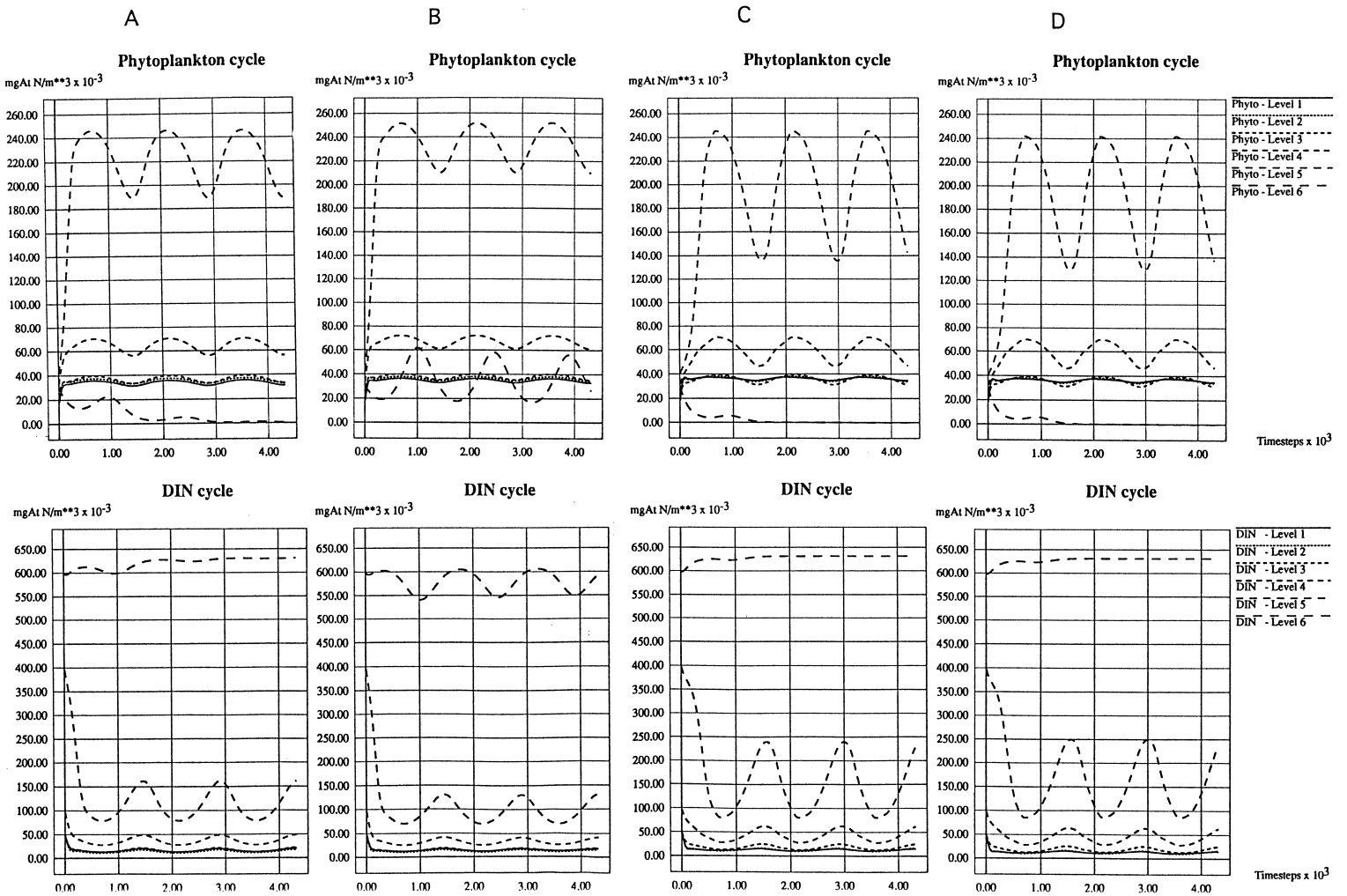

Fig. 4. Concentrations of phytoplankton and dissolved inorganic nitrogen obtained with the standalone NPD model: (a) UNESCO (1983) irradiance; (b) irradiance calculated as in formula label E:NPD; (c) As in (b) plus COADS clouds coverage; (d) As in (c) plus selfshading.

when the oligotrophy is released. The integration of the NPD equation gives the opportunity to numerically investigate the behaviour of the time response of the NPD system (Fig. 4). In these simulations the phytoplankton and DIN concentration evolution is shown at six different levels (5 m, 15 m, 30 m, 50 m, 70 m, 90 m). The initial conditions are the same used in the Ionian Sea initialization of the overall model. Four different irradiance models are considered. The main difference between the UNESCO (1983) and Eq. (9) parameterization of irradiance is essentially the different excursion of the phytoplankton cycle, and this also causes the phytoplankton extinction at 90 m. The introduction of clouds increases the excursion, even with respect to the first case; moreover at 90 m, phytoplankton disappears after the first year. The introduction of selfshading, $k_{\text{phyto}} = 0.3 \times 10^{-3}$ m^2 $mgatN^{-1}$, does not change the patterns and values of the cycle in a significant way. Thus this parameter is not used in the coupled simulations shown in this work, even though further investigations seem to be necessary to assess the importance of selfshading effects in this oligotrophic environment.

3. Simulation results

3.1. Model runs, spinup and quasi repeating cycle

The simulation experiments were planned so as to obtain a quasi-repeating cycle. The MOM-based primitive equation model set up by Pinardi et al. (1993) is run first to obtain the spinup of the hydrodynamics. The version used in this paper, hereafter called PE4L31, has a spatial discretization of 1/4 degree horizontally and 31 levels vertically. The level depths for tracers are located respectively at 5, 15, 30, 50, 90, 120, 160, 200, 240, 280, 320, 360, 400, 440, 480, 520, 580, 660, 775, 925, 1150, 1450, 2050, 2350, 2650, 2950, 3250, 3550, 3850 m.

The subgrid turbulence parametrization is known to be crucial in determining the high frequency tail of the power spectrum as well as the high wavenumber spectra for active and passive tracers. The constant coefficient parametrization adopted in this work was subjected to a sensitivity analysis in the first runs (run b.1, b.2, b.3, not shown), considering also the parametrizations used for similar numerical experiments (Wu and Haines, 1996). The figures obtained represent a good compromise between subbasin scales permanence and model stability: we have 0.4×10^{19} cm^4 s^{-1}, as biharmonic horizontal eddy viscosity, and 1.5 cm^2 s^{-1} for the vertical viscosity, while 0.2×10^{19} cm^4 s^{-1} and 0.3 cm^2 s^{-1} are respectively the biharmonic horizontal and vertical eddy diffusivity coefficients for physical tracers while the omologous for the biological parameters are reported in Table 1.

The spinup of PE4L31 is 5 years with a timestep of 2400 s, chosen as a compromise between asymptotic convergence of the kinetic energy and progressive vertical structure erosion induced by the diffusive processes. After the spinup time the whole coupled model is run for at least 3 years. This time seems enough to reproduce a seasonal cycle in the upper layer. A summary of the most important numerical experiments is presented in Table 2. The first observation to make is that the sensitivity analysis is focused basically on the ecological part. An exception is run b11 which uses higher horizontal eddy viscosity and diffusivity.

In Fig. 5, the relative effects of model sensitivity to the incremental parameter variation are presented in a scatter plot form: in the case of linear correspondence between variables the scatter plot is supposed to lie on a straight line. Two reference levels were

Table 2
Selected numerical experiments with PE4L31-NPD coupled model

Run	PE4L31 model	NPD model
b8.1	standard	standard with $w_D = 0$
b9.567	standard	standard
b10.5678	standard	standard with $w_D = 0.0058$ cm s^{-1} and $r = 1.1810^{-6}$ s^{-1}
b11.567	$A_H = 0.8 \times 10^{19}$	as b10.5678 with $K_H = 0.4 \times 10^{19}$
b14.567	standard	as b10.567 with improved light model

The hydrodynamics has a spinup time of 5 years. The duration of each biological run after the fifth year is indicated in the postfix of each run name. Each run is identified by the key modifications introduced in that run. The standard parameters are those presented in Table 1.

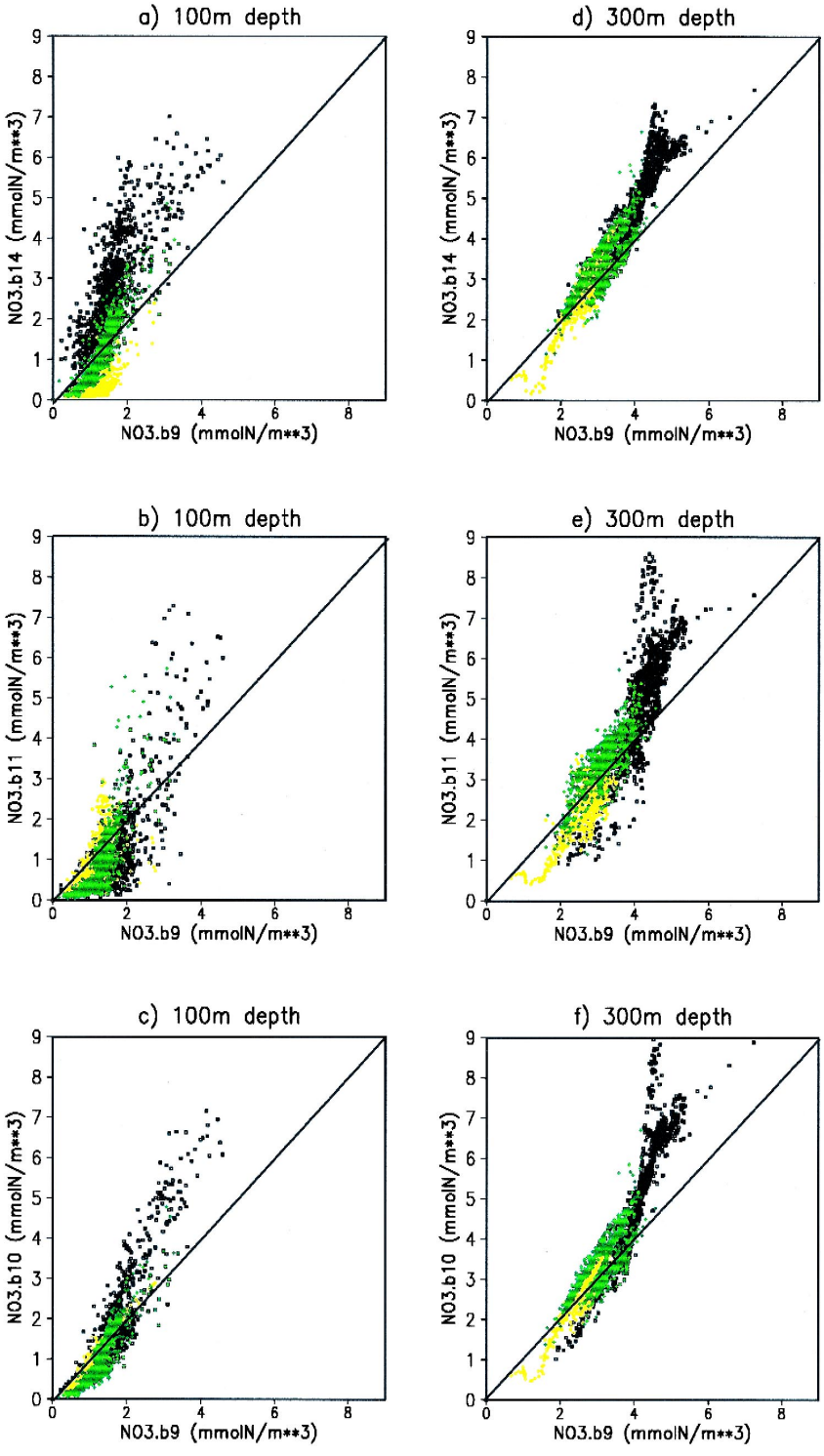
a) 100m depth
NO3.b14 (mmolN/m**3)
NO3.b9 (mmolN/m**3)
d) 300m depth
NO3.b14 (mmolN/m**3)
NO3.b9 (mmolN/m**3)
b) 100m depth
NO3.b11 (mmolN/m**3)
NO3.b9 (mmolN/m**3)
e) 300m depth
NO3.b11 (mmolN/m**3)
NO3.b9 (mmolN/m**3)
c) 100m depth
NO3.b10 (mmolN/m**3)
NO3.b9 (mmolN/m**3)
f) 300m depth
NO3.b10 (mmolN/m**3)
NO3.b9 (mmolN/m**3)

Table 3
Annual nitrate budget estimations in the Gibraltar and Sicily straits (10^6 t yr^{-1})

Nitrate concentrations	Water fluxes	Gibraltar	Sicily
Coste et al. (1988)	Lacombe (1971)	−2.21	–
Coste et al. (1988, Coste (1971)	Béthoux (1979)	−3.11	−1.58
Coste et al. (1988, Coste (1971)	Sarmiento et al. (1988)	−1.25	−0.91
Coste et al. (1988)	Bryden and Kinder (1991)	−1.05	–
Coste et al. (1988, Coste (1971)	Harzallah et al. (1993)	−1.41	−0.85
b8	PE4L31	−1.73	−0.51
b9	PE4L31	−1.78	−0.63
b10	PE4L31	−2.74	−1.85
b14	PE4L31	−2.50	−1.70

The model results are evaluated after the first year of simulation.

chosen to see the differences in model response: one at 100 m depth, where the DIN concentration begins to be evident, and the other at 300 m depth, below the direct effect of the productive layer, and different markers are used to identify the subbasins. The effects of the enhanced vertical flux (run b10) are evident in the increment in DIN concentration both at 100 m (Fig. 5c) and 300 m (Fig. 5f) for the Western Mediterranean. The Ionian Sea does not present any variation while the Levantine seems to be more nutrient depleted. If higher horizontal viscosity and diffusivity are introduced (run b11) the shape of the scatter plot is basically the same, but the marker cloud is much more scattered, both at 100 m and 300 m (Fig. 5b and e, respectively). The spreading is present in all the basins, stronger in the upper level and more pronounced for low concentrations. This effect can be related to the basin-wide constant parametrization of eddy viscosity and diffusivity.

The improved light model has the effect of reducing high concentrations, and this is particularly true at 300 m (Fig. 5d). This is definitely not a direct effect on phytoplankton uptake because the productive layer is shallower in the Western Mediterranean (where the differences are higher) in b14 than in b9. Instead a reduction in solar irradiance during the most productive period (late winter–early spring) reduces the downward fluxes of detritus, limiting the increment of remineralized DIN.

In conclusion, the vertical detritus fluxes seem to play a major role in maintaining the vertical nutrient gradient. Here, we will discuss in particular the results obtained in run b14, which is considered the most detailed in the parametrization of physical forcings and biological response, and all the examples will be referred to this run unless otherwise stated.

3.2. Nitrogen budgets

In Table 3, the total nitrate budgets in the Gibraltar and Sicily straits after the first year of simulation are reported. All the numerical experiments were obtained with the same physical submodel. These results are compared with some estimates obtained in terms of water fluxes and using the nitrate mean concentrations in the inflow and outflow water masses. For nitrate concentrations in the Gibraltar Strait, an inflow mean concentration of 4.0 mgatN m^{-3} and an outflow of 8.6 mgatN m^{-3} are used (Coste et al., 1988). For the Sicily Strait the estimate of 4.0 mgatN m^{-3} for the outflow water concentration is used, while for the inflow an upper value of 1.0 mgatN m^{-3} is held fixed (Coste, 1971).

Fig. 5. Scatter plot of DIN annual means obtained with run b9 vs. b14, b11, and b10 at 100 m (plots a, b and c) and at 300 m (plots d, e, and f) depth, respectively. The Levantine and the Ionian values are marked in yellow and green, the other Mediterranean values are plotted in black.

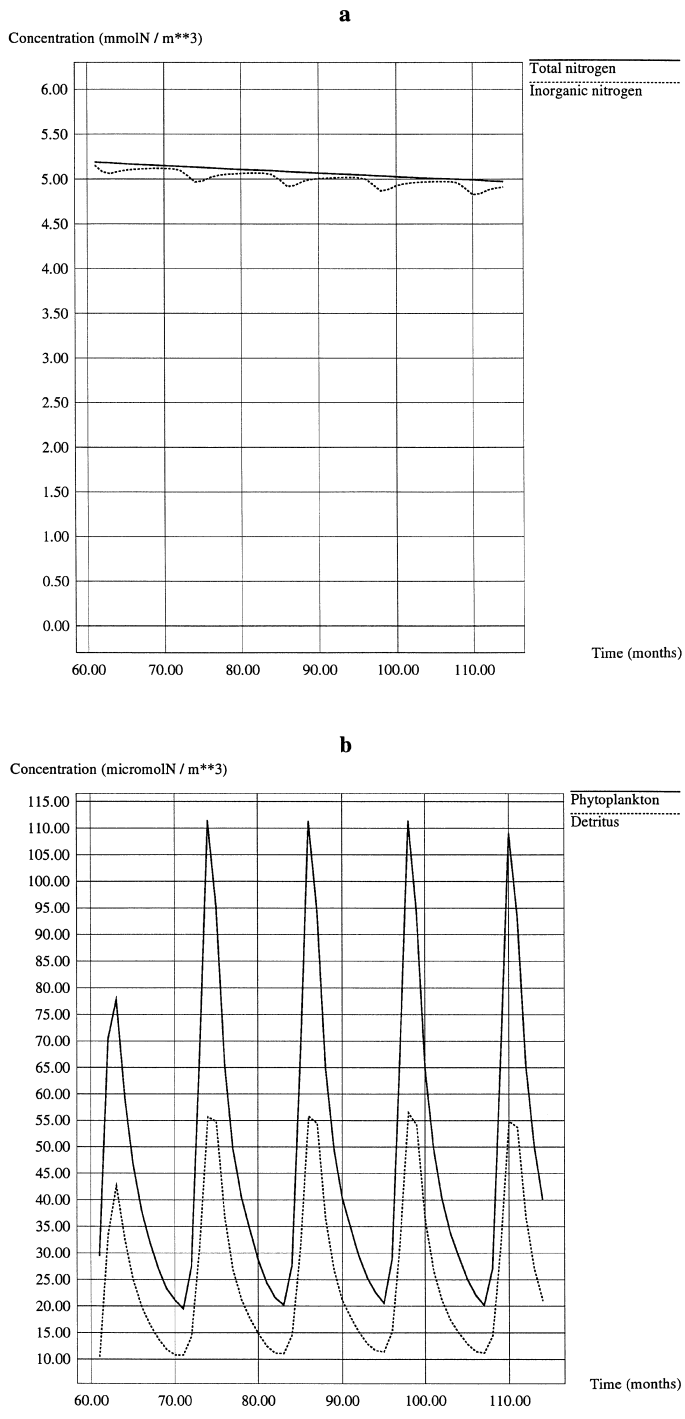

Fig. 6. Seasonal cycle of the basin averaged total and inorganic nitrogen concentrations (mmol N m^{-3}) (a), and phytoplankton and detritus concentrations (μmol N m^{-3}) (b) after 5 years hydrodynamics spinup.

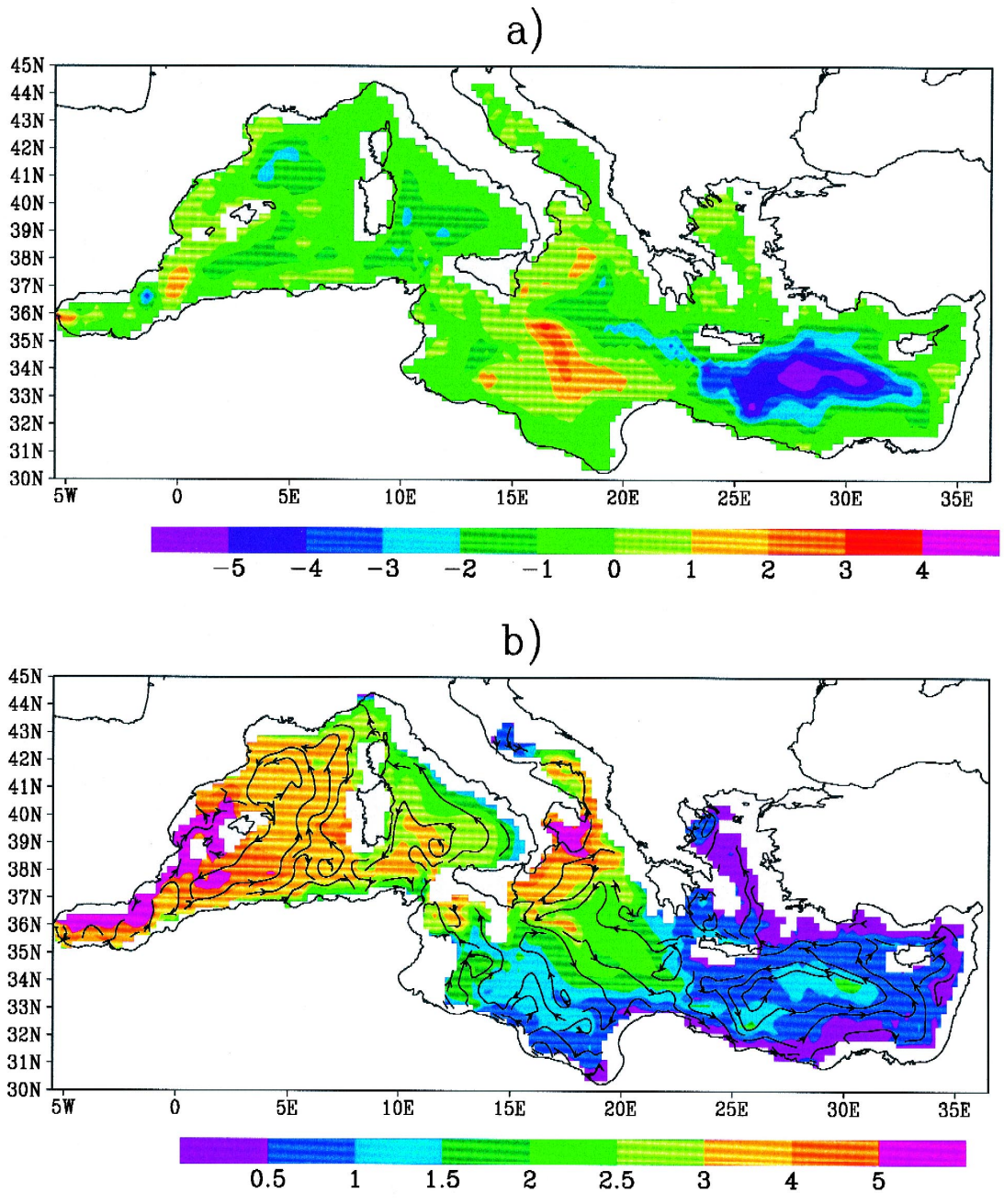

Fig. 7. (a) Annual means of the total transport stream function (Sv); (b) DIN concentration at 140 m (mmol N m^{-3}) superimposed over the streamlines of the velocity vertically integrated above this quota.

The model results are in keeping with the budget estimate ranges here considered. Our lowest results were obtained using no sinking rates (run b8). This is due to the fact that in this run we did not have any mechanism to pump the matter down. Considering a sinking rate of 1 m day^{-1} (run b9), an increased loss at the strait is obtained. This result is magnified by a further increase in the sinking rate and regeneration time (run b10), suggesting that this could be a good choice for calibration of the overall model. Also the introduction of a variable penetration light coefficient diminishes the exchanges and this is due to the lower biological activity in particular in the western part of the basin.

The phytoplankton and the detritus concentrations show, when averaged throughout the basin, a clear seasonal peak in March–April, (Fig. 6b). The monthly sampling prevents the capture of the expected delay in detritus possibly because the time shift is supposed to be smaller than the sampling time. The evolution shown refers to run b10, 54 months of simulation starting from the January initial conditions. The cycle obtained for this run is quasi-stationary in the sense that the late winter maximum and late summer minimum of the phytoplankton and the pattern of evolution are maintained over the 4 years of simulation.

The total and the inorganic nitrogen present, as expected, a negative trend that explains the nutrient net loss at Gibraltar (Fig. 6a). The seasonal cycle is superimposed and seems to be not influenced by the trend, at least during this experiment.

3.3. Climatology

As a climatological synopsis of the trophic response to physical forcings in the Mediterranean Sea we present a comparison between the stream function and the nutrient distribution below the euphotic zone. Fig. 7a represents the annual mean total transport streamfunction ψ expressed in *Sv*; the centers of the anticyclones and the cyclones are identified respectively by positive and negative values. The model reproduces the well known permanent cyclonic patterns in the Gulf of Lions, in the Thyrrenian, and in the Levantine Basin. The Algerian current is represented by the presence of an unstable coastal front that on average exhibits an energetic sequence of cyclonic and anticyclonic gyres. In the Ionian Sea we find that the circulation is basically anticyclonic, but the center of the basin is directly influenced by a wind-driven cyclonic gyre. The Levantine basin is influenced by the large cyclonic area connected with the Rhodes gyre, with the noticeable exception of the anticyclone offshore from the Israeli coast.

If we compare the above maxima and minima positions with the maxima in DIN concentration at 140 m depth (Fig. 7b), where no primary production is present, we see that there is a strong correlation between the high nutrient concentration spots and cyclonic areas in the open sea, while coastal effects such as upwellings and coastal boundary currents are the prevailing processes in importing nutrients into areas such as the Spanish coast of the Alboran Sea, the Sicily and Calabria coasts, and the Algerian current. On the contrary, the effect of the anticyclonic areas on the DIN distribution is less evident in the upper layer because the Ekman pumping in an anticyclonic vortex deepens the nutrient depleted layer, advecting water laterally in the upper layer. This effect can increase the spreading of coastal upwellings and possibly contributes to the remote control of the straits regime (in particular in the Ionian sea).

The permanent cyclonic gyres in the Gulf of Lions and in the Rhodes area create isopycnal domes that carry nutrients into the euphotic zone, substaining the nutrient maxima reproduced by the model. This effect is also present in the Thyrrenian, but is much smoother.

In order to give a comprehensive view of the correlation between general circulation and DIN distribution, we plotted in Fig. 8 the stream function vs.

Fig. 8. Scatter plot of total transport streamfunction (Sv) in abscissa vs. DIN concentration (mmol N m^{-3}) in ordinates respectively at 40 m (a), 100 m (b), 180 m (c) and 300 m (d) depth. With lb and gl, we denote the DIN concentrations coming from Levantine Basin and Gulf of Lions areas.

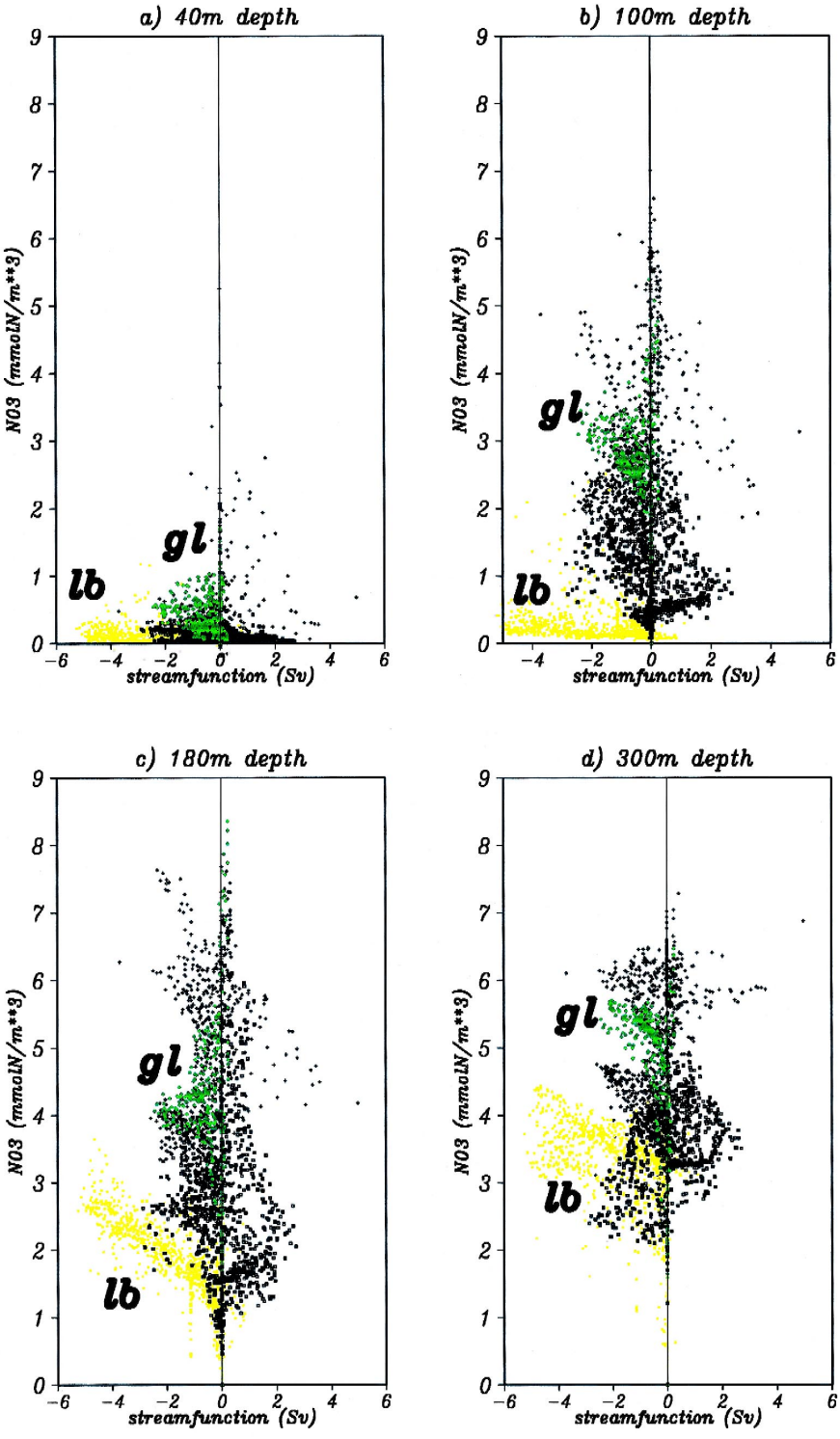
a) 40m depth
b) 100m depth
c) 180m depth
d) 300m depth
NO3 (mmolN/m**3)
streamfunction (Sv)
gl
lb
0
1
2
3
4
5
6
7
8
9
−6
−4
−2
0
2
4
6

nutrient concentration at different depths using yellow for the Levantine Basin, green for the Gulf of Lions (lb and gl in the figure) and black markers for the rest of the Mediterranean.

In Fig. 8a, we see that at 40 m depth there is virtually no effect of the circulation on nutrient distribution and the highest maxima are present in proximity to $\psi = 0$, a condition found along the coasts, suggesting that the upwelling areas could be the main origin of this maximum. This effect is present, with different intensities in all the plots in Fig. 8.

Neither the Levantine nor the Gulf of Lions present a specific response to the cyclonic circulation: this can be explained by the fact that the phytoplankton uptake is fast and virtually all new nutrient inputs are transformed into new production. This signal is present in the phytoplankton distribution (not shown).

At 100 m depth (Fig. 8b), we observe a much more scattered distribution and this is due to two concurring causes: the progressive increase in nutrient concentration with depth extends the dynamic range of DIN, and the deep chlorophyll maximum (DCM) found around this level in the Levantine basin (Kimor et al., 1987; Krom et al., 1993; Berland et al., 1988), while the Western Mediterranean has a shallower euphotic zone. In the latter case, the phytoplankton uptake is not present and the nutrient distribution is affected only by the physical dynamics and by the remineralization processes. A clear influence of the circulation is therefore expected. The results confirm these speculations: the Levantine Basin has a distribution similar to the previous case, while in the Gulf of Lions the effect of the cyclonic regime begins to be detectable. The anticyclonic circulation does not seem to affect nutrient distribution coherently and this supports the above considerations.

At 180 m and 300 m depth (Fig. 8c and d) we find similar patterns for the basin overall, and in particular no specific influence of the anticyclonic circulation, or dependence of DIN concentration on circulation intensity in both the considered cyclonic areas. The distributions in the lb and gl areas are between the axis $\psi = 0$ and a maximum value proportional to ψ intensity. This effect could be related to homogenization in vortices (Young and Rhines, 1982; Young, 1983), summed with the diffusion introduced to parametrize the subgrid scale mixing effects, these two processes thus working to smooth the DIN gradient induced by circulation. As a net effect we find similar DIN concentrations in the neighbourhoods of the cyclonic gyres even in the presence of high ψ gradients.

Another relevant conclusion is that the distribution of DIN in the upper ocean exhibits a pronounced gradient between western and eastern basin, as demonstrated by nitrates data.

3.4. Seasonal cycle

The trophic seasonal variability in the Mediterranean seems to mitigate the chronic oligotrophy that affects this basin, as seen in Fig. 9a where the DIN distributions at 60 m are shown. In the upper layer where the effect of Ekman suction is stronger, we see that, despite highly different concentrations in the eastern and western basins, in February, the mixing induced by wind stirring and by convective adjustment during the winter season creates large areas with relatively higher nutrient availability. The Ligurian–Provençal Sea and the Catalan Sea seem to be particularly involved in these processes, with a southern zonal front roughly corresponding to the Balearic Front (Millot, 1987). The Ligurian Sea seasonal cycle will be compared against a pelagic water column dataset in the CCM-2 confirming the basic seasonal behaviour. Strong wind driven upwellings are present at the northern coast of the Alboran Sea and along the Provençal and Catalan coasts. In the Alboran sea, there is a signature of fronts produced by the Western and Eastern (weaker) Alboran Gyres. The Mediterranean water flowing along the Spanish coast, enriched in nutrients by coastal processes, exhibits higher nitrate concentrations than the surface Atlantic water at the same level. This is in accord with the ALMOFRONT 1 experimental results of Prieur and Sournia (1994). The prevailing northwesterly winds create upwelling along the south-western Sicily coast and along the Calabrian coast. The Levantine Basin attains its highest DIN concentration in this month, possibly because of the dense water formation and the instability that eventually generate a vertical homogenization dragging on the surface nutrients present at depth. There is also

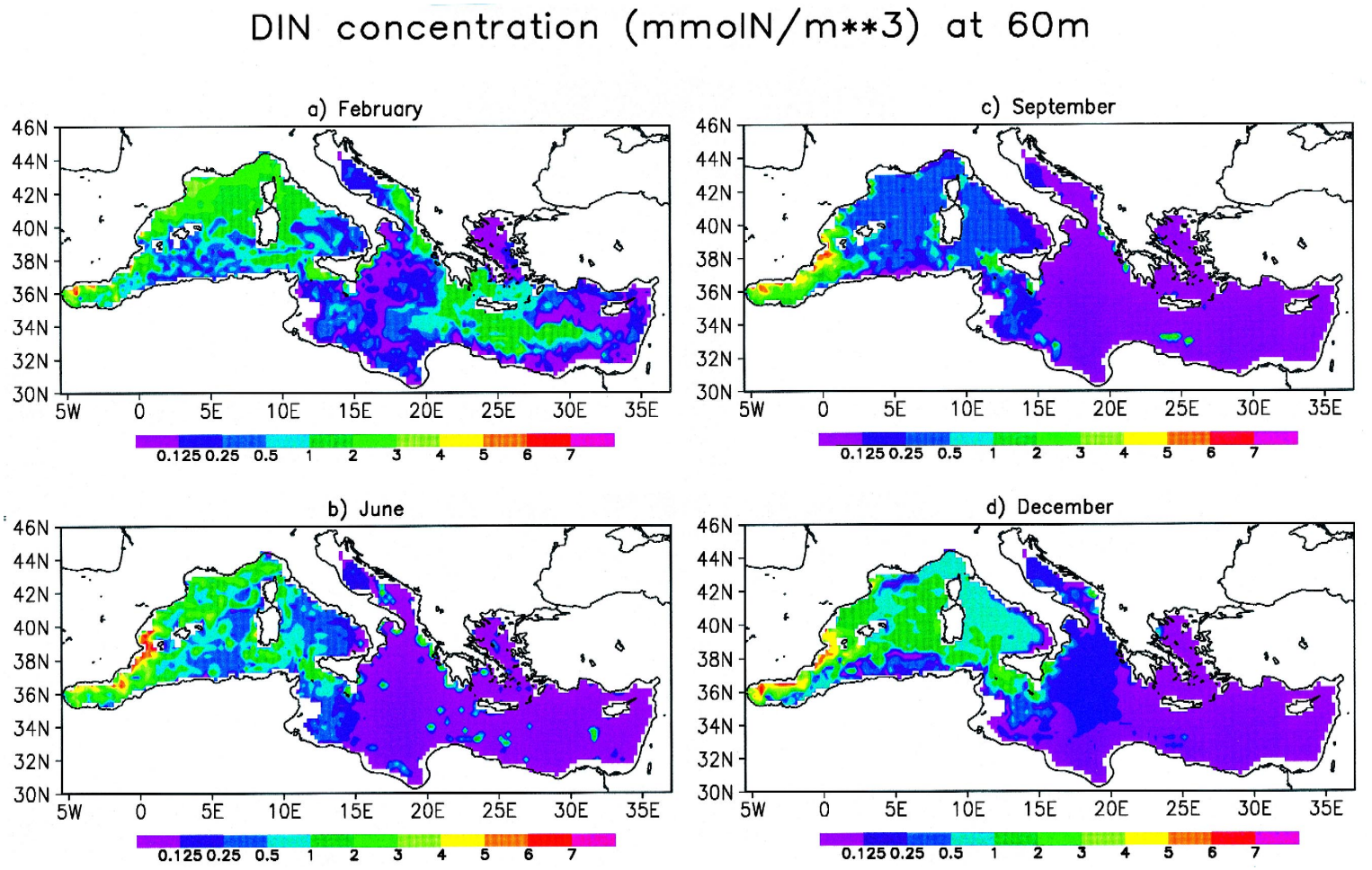

Fig. 9. DIN distributions in February (a), June (b), September (c) and December (d) at 60 m depth (mmol N m^{-3}).

a) NO3 concentration at 8E 42N

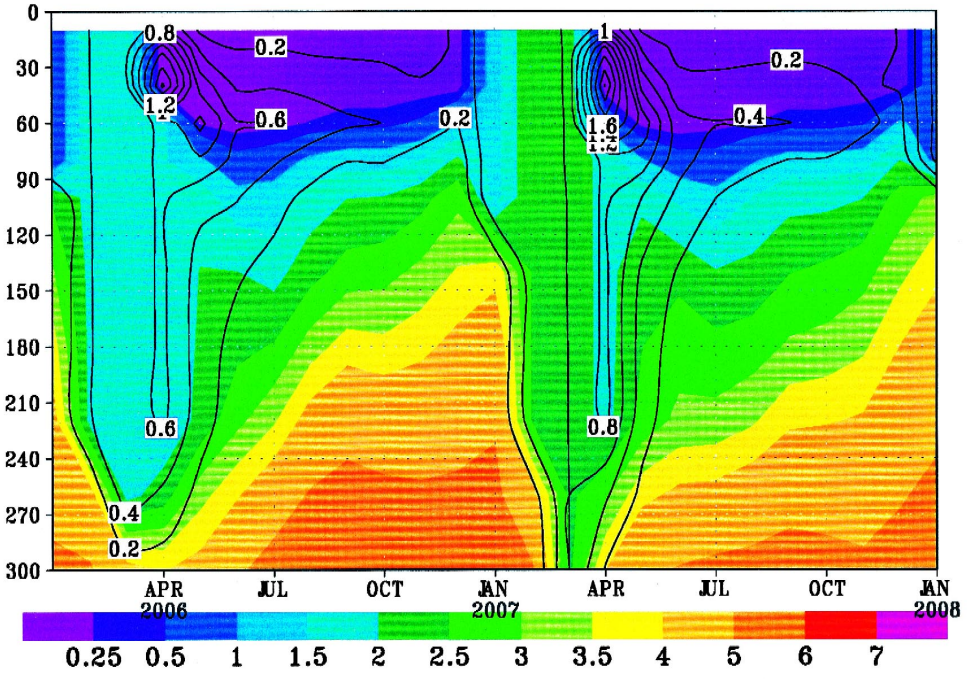

b) NO3 concentration at 19E 38N

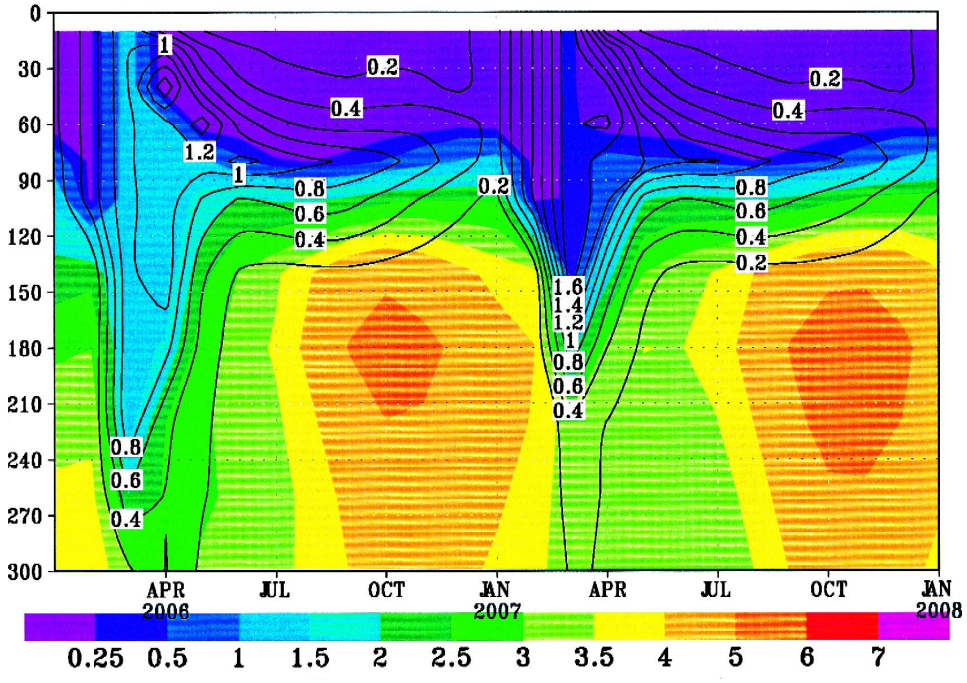

an increased concentration of DIN in the side lobes of the Rhodes Gyre. In June (Fig. 9b) the difference between the two main subbasins is striking and can be related to the different regimes at this level: in the Eastern Mediterranean the nutrient limitation is stronger, because an earlier developed and more stratified seasonal thermocline decouples the upper layer from the ocean interiors, and prevents the input of turbulent energy below the mixed layer. As we can see in Fig. 10b, the 60 m depth level is situated below the thermocline, but because of the high light penetration in this basin the nutricline is located well below this quota. During the relatively calm season this stable vertical structure prevents any trophic input to the nutrient limited upper layer (at least at the climatological scale). These considerations will be verified with an in situ time series in CCM-2.

The above considerations are not valid for the western basin: in this area the light extinction coefficient is higher and the euphotic zone is shallower: Fig. 10a suggests that the 60 m level is on the nutricline edge, explaining the higher concentrations found. In general, the Western Mediterranean exhibits a more energetic distribution of nutrients induced by the wind stress in coastal areas and by the local circulation (Alboran Gyres). High DIN concentrations are present in the Ligurian–Provenccal Basin, maintaining the meridional DIN gradient in this area. The wind driven upwelling offshore from the southern Sicily coast is still present as also shown by Piccioni et al. (1988) using NOAA7 thermal maps for the summer season.

In September (Fig. 9c), the nutrient depletion is still stronger and the map shows a very similar situation to June, with the exception that the Ligurian–Provenccal nutrient concentration is almost homogeneous.

In December (Fig. 9d), the wind and thermohaline forcings cooperate in breaking the thermocline in the western basin, with subsequent mixing; this is not true for the Eastern Mediterranean where late summer conditions are still present. In the Gulf of Lions, low concentrations indicate weak convective adjustments that are only able to mix the upper layer. To explain this fact, let us denote by $z\mathrm{mix}$ the mixing depth and by $\mathrm{DIN}(z)$ the local average DIN concentration at the reference level z; the convective adjustment can be seen as an infinite velocity vertical mixing which affects the physical and biological tracers. $DIN(z)$ can be described as continuous function monotonically increases with depth within the mixing length, as we can safely assume since the biologically mediated depletion of the euphotic zone contributes to maintain a well shaped nutricline. We obtain that, after convection, the average (vertically homogeneous) DIN concentration is:

$$\overline{DIN} = \frac{1}{z\mathrm{mix}} \int_0^{z\mathrm{mix}} DIN(z)\,\mathrm{d}z$$

which will be comprised between by $\mathrm{DIN}(0)$ and $\mathrm{DIN}(z\mathrm{mix})$ (average theorem).

$$DIN(0) < \overline{DIN} < DIN(z\mathrm{mix})$$

At the $z\mathrm{mix}$ depth, thus, the convection affected area will experience a reduction of nutrient (conversely at surface).

In this season, the Algerian Current seems to be more energetic, but its contribution in terms of nutrients is negligible. The Ionian Sea, however, seems to be nearer to winter conditions when increased nutrient availability is present, in particular in the northern part of the basin.

In Fig. 11, four DIN monthly maps at 180 m are presented. In February, the signature of the vertical homogenization in the Liguro–Provenzal Basin and in the Cretan Passage is seen by comparing Fig. 9a and Fig. 11a we notice at these two sites that the same area has the same DIN concentration (darker in Fig. 9a and lighter in Fig. 11a). The intense vertical export of nutrients from ocean interiors and the enhanced wind driven circulation determine a patchy trophic distribution.

During the early summer and late autumn periods, a progressive DIN replenishment occurs, finally producing a nutrient pool for the next winter mixing

Fig. 10. Second and third year time-depth diagrams in two sample station in Western (a) and Eastern (b) Mediterranean for inorganic nitrogen (shaded) and phytoplankton (contoured), both in mmol N m^{-3}. The year 2000 is assumed as the conventional starting time.

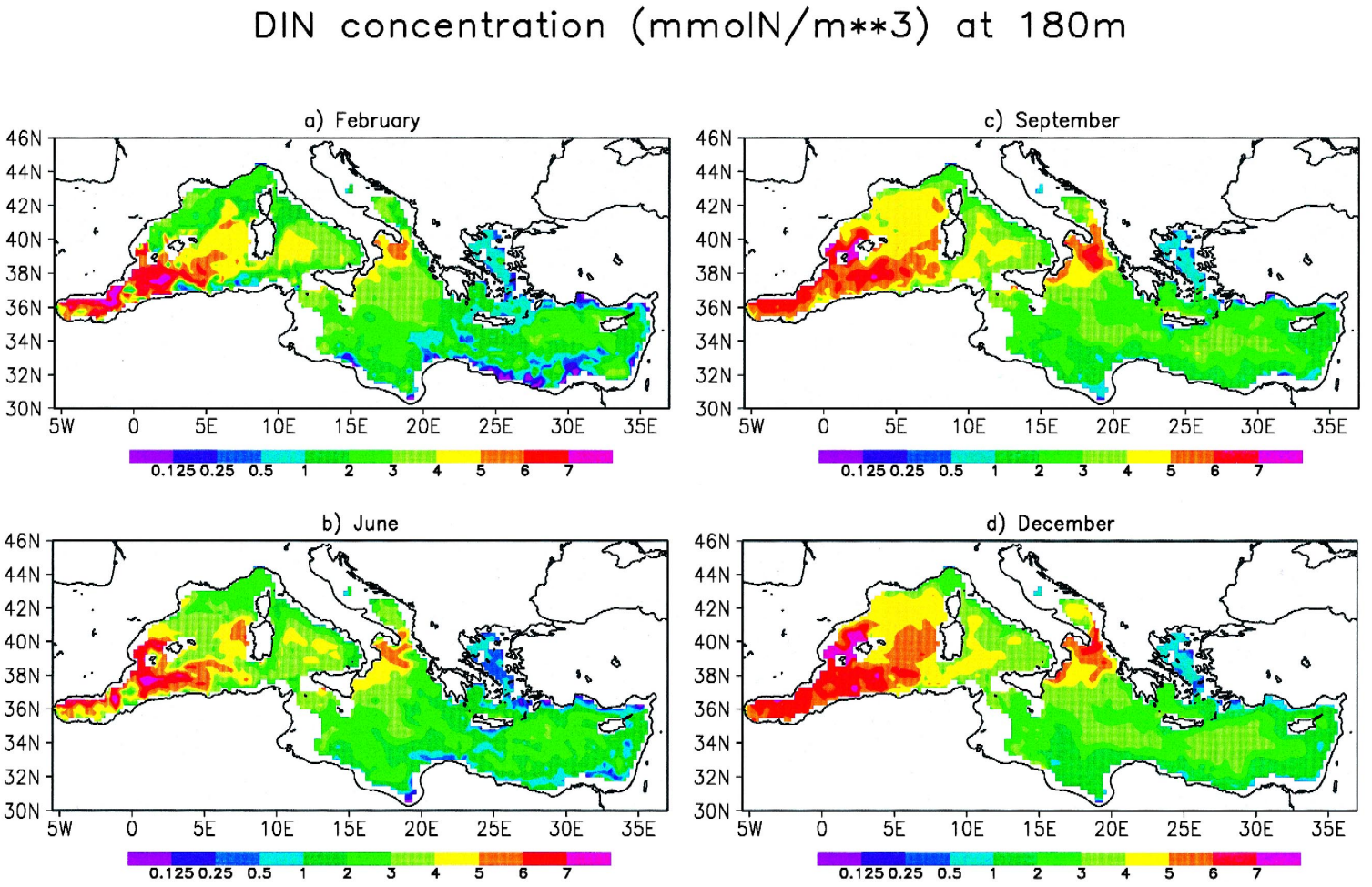

Fig. 11. DIN distributions in February (a), June (b), September (c) and December (d) at 180 m depth (mmol N m^{-3}).

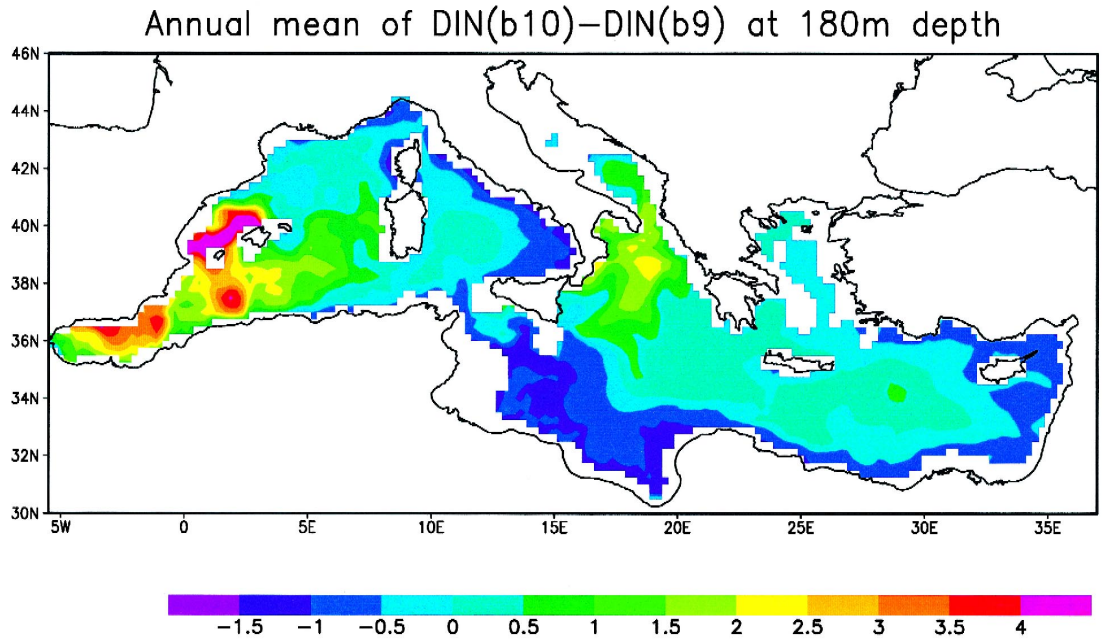

Fig. 12. Annual mean of the difference of the DIN concentration at 180 m depth between b10.567 (high detritus flux) and b9.567 (low detritus flux) expressed in mmol N m^{-3}.

period. In this process, the vertical flux induced by the detritus sinking can be estimated, showing the difference in DIN concentration below the nitracline (180 m) between the b9 and b10 runs (Fig. 12), which differ for detritus sinking velocities and remineralization rate parametrizations (see Table 2). The b10 experiment allows higher nutrient regeneration in depth, where higher primary production and higher standing stocks are present. This in turn allows the presence of a seasonally varying detritus vertical flux that induces fertilization of the layers below the nitracline during spring and summer, thus creating an enriched pool of biochemical energy. This forms a trophic cell able to capture the nitrogen forms and to maintain lateral inhomogeneities over time, even in the presence of intense lateral advection (as in the Alboran Sea).

4. Discussion

Analysis of the model results leads to the conclusion that the main influence of the general circulation on the Mediterranean ecosystem functioning is related to nutrient horizontal and vertical transport. At the climatological scale, the general circulation induces two different trophic regimes in the two principal subbasins, due to the combined effect of the estuarine inverse circulation and the impact of all the biogeochemical processes involved in degradation of the organic matter. The nitrogen budget of the two basins is very sensitive to the remineralization rate and detrital sinking velocity, particularly in the Eastern Mediterranean. In light of this result, a thorough estimation of the energy dissipated in the vertical and horizontal diffusion processes is an important step in the calibration of this three-dimensional model.

Moreover, the cyclonic areas exhibit less oligotrophy than their surroundings, while the anticyclones maintain the nutrient depleted characteristics of the productive layer in depth, not substantially modifying the ecosystem response.

The seasonal cycle in Mediterranean Sea is basically driven by physical forcings: the combined effect of the mixed layer dynamics and the seasonal

fluctuation of the irradiance determines different responses according to the trophic regime (basically nutrient limited at surface, with the important exception of the winter period, and light limited in depth). The key features are captured in the NPD formulation of the trophodynamic model, supporting the idea that the vertical dynamics of the mid-latitude ecological systems can be explained, to a first approximation, as being driven by the combined effect of the mixed layer dynamics and the irradiance annual signal (Valiela, 1995). Our aggregate model is able to automatically adjust to the different situations present during the seasonal cycle in the Mediterranean from winter (vertical mixing, relatively high nutrient availability, fair irradiance) to summer (stratification, nutrient depletion, high irradiance), giving conditions for phytoplankton persistence consistent with other independent considerations. Advection and diffusion processes contribute to deeply modify the vertical dynamics, creating and maintaining spatial gradients, in particular for DIN (notably westward but also northward). These processes are mainly explained in terms of general circulation.

The comparison of model results with experimental data is presented in CCM-2, suggesting that the NPD formulation can explain nitrogen seasonal cycles in the open Mediterranean Sea, according to the prevailing cyclonic or anticyclonic regimes and to the zonal and meridional permanent trophic gradients, and resolves the basin-wide spatial and temporal gradients in surface chlorophyll.

These results are corroborated by those obtained through a similar model (Hurtt and Armstrong, 1996), calibrated against the Bermuda Atlantic Time Series data set. Further development of the ecological model structure is needed, but analogous Mediterranean data sets should be made available for calibration and verification.

Acknowledgements

This work was partially funded by the EC contract Mediterranean Eddy Resolving Modelling And InterDisciplinary Studies-II (MAS2-CT93-0055). The authors wish to thank Nadia Pinardi for suggestions and for supplying the hydrodynamical models and Valentina Mosetti for computer management of the OGS ECHO group. All the color figures were obtained with the public domain package GrADS.

References

Anderson, T.R., Andersen, V., Fransz, H.G., Frost, B.W., Klepper, O., Rassoulzadegan, F., Wulff, F., 1993. Modelling zooplankton. In: Evans, G.T., Fasham, M.J.R. (Eds.), Towards a Model of Ocean Biogeochemical Processes. Springer-Verlag, pp. 177–191.

Armstrong, R.A., 1994. Grazing limitation and nutrient limitation in marine ecosystems: steady-state solutions of an ecosystem model with multiple food chains. Limnol. Oceanogr. 39, 597–608.

Azov, Y., 1986. Seasonal patterns of phytoplankton productivity and abundance in nearshore oligotrophic waters of the Levant Basin abundance in nearshore oligotrophic waters of the Levant Basin (Mediterranean). J. Plankton Res. 8 (1), 41–53.

Baretta, J.W., Ebenhöh, W., Ruardij, P., 1995. The European Regional Seas Ecosystem Model, a complex marine ecosystem model. Neth. J. Sea Res. 33 (3–4), 233–246, Special issue.

Berman, T., Azov, Y., Schneller, A., Walline, P., Townsend, D.W., 1986. Extent, transparency, and phytoplankton distribution of the neritic waters overlying the Israeli coastal shelf. Oceanol. Acta 9 (4), 439–447.

Berland, B.R., Benzhitski, A.G., Burlakova, Z.P., Georgieva, L.V., Izmestieva, M.A., Khodolov, V.I., Maestrini, S.Y., 1988. Condition hydrologiques estivales en Méditerranée, répartition du phytoplankton et la matière organique. Oceanol. Acta 9 (1988), 163–177, Special issue.

Béthoux, J.P., 1979. Budgets of the Mediterranean Sea. Their dependance on the local climate and on the characteristics of the Atlantic waters. Oceanol. Acta 2 (2), 157–163.

Bryden, H., Kinder, T.H., 1991. Steady two-layer exchange through the Strait of Gibraltar. Deep-Sea Res. 38, 445–463, Suppl. 1.

Brock, T.D., 1981. Calculating solar radiation for ecological. Ecol. Model. 14, 1–19.

Broekhuizen, N., Heath, M.R., Hay, S.J., Gurney, W.S.C., 1995. Modelling the dynamics of the North Sea's mesozooplankton. Neth. J. Sea Res. 33 (3–4), 381–406, Special issue.

Castellari, S., Pinardi, N., Navarra A., 1990. A realistic General Circulation Model of the Mediterranean Sea: I. Surface energy parametrization and meterological forcing dataset. IMGA-CNR Tech. Report, pp. 4–90.

Coste, B., 1971. Le sels nutritifs entre la Sicilie, la Sardaigne et la Tunisie. Cah. Océanogr. 23, 49–83.

Coste, B., Gostan, J., et Minas, H.J., 1972. Influence des Conditions Hivernales sur les productions Phyto- et Zooplanctoniques en Méditerranée Nord-Occidentale: I. Structures hy-

drologiques et distribution des sels nutritifs. Mar. Biol. 16, 320–348.

Coste, B., Le Corre, P., Minas, H.J., 1988. Re-evaluation of the nutrient exchanges in the Strait of Gibraltar. Deep-Sea Res. 35, 767–775.

Crise, A., Crispi, G., Mosetti, R., 1992. Parallelization of a coupled hydrodynamical ecomodel. CNR/PFI, Tech. Report No. 135, p. 20 + fig. 8.

Crispi, G., Crise, A., Mauri, E., 1999. A seasonal three-dimensional study of the nitrogen cycle in the Mediterranean Sea: II. Verification of an energy constrained trophic model. J. Mar. Syst. in press.

Eppley, R.W., 1972. Temperature and phytoplankton growth in the sea. Fish. Bull. 70, 1063–1085.

Eppley, R.W., Peterson, B.J., 1979. Particulate organic matter flux and planktonic new production in the deep ocean. Nature 282, 677–680.

Fasham, M.J.R., Ducklow, H.W., McKelvie, S.M., 1990. A nitrogen-based model of plankton dynamics in the oceanic mixed layer. J. Mar. Res. 48, 591–639.

Fasham, M.J.R., Sarmiento, J.L., Slater, R.D., Ducklow, H.W., Williams, R., 1993. Ecosystem behavior at bermuda station 'S' and ocean weather station 'India': a general circulation model and observational analysis. Global Biogeochem. Cycles 7 (2), 379–415.

Forsythe, W.C., Rickel, E.J. Jr., Sthal, R.S., Wu, H., Schoolfield, R.M., 1995. A model comparison for daylength as a function of latitude and day of the year. Ecol. Model. 80, 87–95.

Fransz, H.G., Mommaerts, J.P., Radach, G., 1991. Ecological modelling of the North Sea. Neth. J. Sea Res. 28, 67–140.

Gould, R.W. Jr., Wiesenburg, D.A., 1990. Single-species dominance in a subsurface phytoplankton concentration at a Mediterranean Sea front. Limnol. Oceanogr. 35 (1), 221–230.

Harzallah, A., Cadet, D.L., Crepon, M., 1993. Possible forcing effects of net evaporation, atmospheric pressure, and transients on water transports in the Mediterranean Sea. J. Geophys. Res. 98 (C7), 12341–12350.

Hurtt, G.C., Armstrong, R.A., 1996. A pelagic ecosystem model calibrated with BATS data. Deep-Sea Res. II 43 (2–3), 653–683.

Kimor, B., Berman, T., Schneller, A., 1987. Phytoplankton assemblages in the deep chlorophyll maximum layers off the Mediterranean coast of Israel. J. Plankton Res. 9 (3), 433–443.

Krom, M.D., Brenner, S., Kress, N., Neori, A., Gordon, L.I., 1993. Nutrient distributions during an annual cycle across a warm-core eddy from the E. Mediterranean Sea. Deep-Sea Res. 40 (4), 802–825.

Kovacevic, V., Manca, B., Michelato, A., Scarazzato, P., 1994. DATA REPORT Cruise POEM-BC—October 1991—Ionian Basin and Sicily Strait: I. Hydrological and CTD Data. Tech. Report No. 2/94-OGA-1.

Lacombe, H., 1971. Le détroit de Gibraltar, océanographie physique. Notes Mém. Serv. Géol. Maroc, 222 bis, pp. 111–146.

MacIsaac, J.J., Dugdale, R.C., 1969. The kinetics of nitrate and ammonia uptake by natural populations of marine phytoplankton. Deep-Sea Res. 16, 45–57.

Mann, K.H., Lazier, J.N.R., 1991. Dynamics of Marine Ecosystems. Blackwell, Oxford, 466 pp.

Mauri, E., Crise, A., 1995. The organic nitrogen fluxes. OGS Tech. Report REL. 92/95-OGA, 10, 24 pp.

McGill, D.A., 1970. Mediterranean Sea Atlas—distribution of nutrient chemical properties. Woods Hole Oceanographic Institution, Woodshole, MA.

Millot, C., 1987. Circulation in the western Mediterranean. Oceanol. Acta 10 (2), 143–149.

Najjar, R.G., Sarmiento, J.L., Toggweiler, J.R., 1992. Downward transport and fate of organic matter in the ocean: simulations with a general circulation model. Global Biogeoch. Cycles 6 (1), 47–76.

Osborne, J., Swift, J., Feinchem, E.P., 1992. Ocean Atlas for Macintosh. 106 pp.

Piccioni, A., Gabriele, M., Salusti, E., Zambianchi, E., 1988. Wind-induced upwellings off the southern coast of Sicily. Oceanol. Acta 11 (4), 309–314.

Pinardi, N., Roether, W., Marshall, J., Lascaratos, A., Krestenitis, Y., Haines, K., 1993. Mediterranean eddy resolving modelling and inter disciplinary studies (Contract MAST 0039-C(A)). Final Scientific and Management Report, p. 45.

Poulain, P.-M., Gačić, M., Vetrano, A., 1996. Current measurements in the Strait of Otranto reveal unforeseen aspects of its hydrodynamics. EOS Trans. 77 (36), 345–348.

Prieur, L., Sournia, A., 1994. 'Almofront-1' (April–May 1991): an interdisciplinary study of the Almeria-Oran geostrophic front, SW Mediterranean Sea. J. Mar. Syst. 5 (3–5), 187–203.

Rabitti, S., Civitarese, G., Ribera, M., 1994. Data Report Cruise POEM-BC—October 1991—Ionian Basin and Sicily Channel: II. Chemical and Biological Data. Tech. Report No. 13/94-CNR/IBM.

Redfield, A.C., Ketchum, B.H., Richards, F.A., 1963. The influence of sea water. In: Hill, M.N. (Ed.), The Sea, Vol. 2. Interscience, pp. 26–77.

Reed, R.K., 1977. An estimation of net long-wave radiation from the oceans. J. Geophys. Res. 81, 5793–5794.

Sarmiento, J.L., Herbert, T., Toggweiler, J.R., 1988. Mediterranean nutrient balance and episodes of anoxia. Global Biogeoch. Cycles 2 (4), 427–444.

Sarmiento, J.L., Slater, R.D., Fasham, M.J.R., Ducklow, H.W., Toggweiler, J.R., Evans, G.T., 1993. A seasonal three-dimensional ecosystem model of nutrient cycling in the North Atlantic euphotic zone. Global Biogeoch. Cycles 7 (2), 417–450.

Slagstad, D., 1982. A model of phytoplankton growth-effects of vertical mixing and adaptation to light. Modeling, Identification and Control 3 (2), 111–130.

Steele, J.H., 1962. Environmental control of photosynthesis in the sea. Limnol. Oceanogr. 7, 137–150.

Tusseau, M.H., Mouchel J.-M., 1995. Nitrogen inputs to the Gulf of Lions via the Rhone river. In: Martin, J.M., Barth, H. (Eds.), EROS 2000 Fifth Workshop on the North-West Mediterranean Sea. Report EUR 16130 EN, pp. 49–60.

UNESCO, 1983. Quantitative analysis and simulation of Mediterranean coastal ecosystem: the Gulf of Naples, a case study. UNESCO Rep. Mar. Sci. 20, 158.

Valiela, I., 1995. Marine Ecological Processes. Springer, Berlin, p. 686.

Wu, P., Haines, K., 1996. Modeling the dispersal of levantine intermediate water and its role in Mediterranean deep water formation. J. Geophys. Res. 101 (C3), 6591–6607.

Young, W.R., 1983. The role of western boundary layer in gyre-scale ocean mixing. J. Phys. Oceanogr. 14, 478–483.

Young, W.R., Rhines, P.B., 1982. A theory of the wind-driven circulation: II. Gyres with western boundary layers. J. Mar. Res. 40, 849–872.